High statistics measurement of K_{e4} decay properties

S. Pislak,[1,2] R. Appel,[2,3] G. S. Atoyan,[4] B. Bassalleck,[5] D. R. Bergman,[2,*] N. Cheung,[3] S. Dhawan,[2] H. Do,[2] J. Egger,[6] S. Eilerts,[5,†] H. Fischer,[5,‡] W. Herold,[6] V. V. Issakov,[4] H. Kaspar,[6,2] D. E. Kraus,[3] D. M. Lazarus,[7] P. Lichard,[3] J. Lowe,[5] J. Lozano,[2,§] H. Ma,[7] W. Majid,[2,‖] A. A. Poblaguev,[4] P. Rehak,[7] A. Sher,[3,¶] Aleksey Sher,[1] J. A. Thompson,[3] P. Truöl,[1,2] and M.E. Zeller[2]

[1]*Physik-Institut, Universität Zürich, CH-8057 Zürich, Switzerland*
[2]*Physics Department, Yale University, New Haven, Connecticut 06511*
[3]*Department of Physics and Astronomy, University of Pittsburgh, Pittsburgh, Pennsylvania 15260*
[4]*Institute for Nuclear Research of Russian Academy of Sciences, Moscow 117 312, Russia*
[5]*Department of Physics and Astronomy, University of New Mexico, Albuquerque, New Mexico 87131*
[6]*Paul Scherrer Institut, CH-5232 Villigen, Switzerland*
[7]*Brookhaven National Laboratory, Upton, New York 11973*

(Received 31 January 2003; published 28 April 2003)

We report experimental details and results of a new measurement of the decay $K^+ \to \pi^+ \pi^- e^+ \nu_e (K_{e4})$. A sample of more than 400,000 K_{e4} events with low background has been collected by Experiment 865 at the Brookhaven Alternate Gradient Synchrotron. From these data, the branching ratio $(4.11 \pm 0.01 \pm 0.11) \times 10^{-5}$ and the $\pi\pi$ invariant mass dependence of the form factors F, G, and H of the weak hadronic current as well as the phase shift difference $\delta_0^0 - \delta_1^1$ for $\pi\pi$ scattering were extracted. Using constraints based on analyticity and chiral symmetry, a new value with considerably improved accuracy for the s-wave $\pi\pi$ scattering length a_0^0 has been obtained also: $a_0^0 = 0.216 \pm 0.013$ (stat) ± 0.002 (syst) ± 0.002 (theor).

DOI: 10.1103/PhysRevD.67.072004 PACS number(s): 13.20.Eb, 13.75.Lb

I. INTRODUCTION

Among the long list of possible charged kaon decays the rare K_{e4} decay branch $[K^\pm \to \pi^+ \pi^- e^\pm \nu_e(\bar{\nu}_e)]$ has received particular attention because it was recognized [1] almost coincidently with the observation of the first event for this decay 40 years ago [2] that it could provide important information on the structure of the weak hadronic currents and also on $\pi\pi$ scattering at low energies. The final state interaction of the two pions was expected to manifest itself in an angular correlation between the decay products, namely an asymmetry of the lepton distribution with respect to the plane formed by the two pion momenta. This asymmetry is directly related to the difference between the s- and p-wave scattering phase. What made this four-body semileptonic decay attractive despite its low branching ratio, which was then predicted to be of order 10^{-5} [3], is that the two pions are the only hadrons in the final state. For all other reactions used to study the $\pi\pi$ interaction, e.g. $\pi^- p \to \pi^- \pi^+ n$, there is at least one other hadron present in the final state. Thus experimental studies of the K_{e4} decay were seen as the cleanest method to determine the isospin zero, angular momentum zero scattering length a_0^0. Since early experiments [4–8] observed only a few hundred events each, it was not until 1977, when the Geneva-Saclay experiment [9] gathered about 30,000 events, that a measurement was made of this quantity to 20% accuracy.

Since then no new data became available until Experiment 865 at the Brookhaven Alternating Gradient Synchrotron collected 400,000 K_{e4} events. We report here the details of the analysis of these data, some of which have been communicated earlier [10]. A promising alternative way to study $\pi\pi$ interactions through a measurement of the lifetime of the $\pi\pi$ atom is followed in the DIRAC experiment at CERN [11], which has not yet yielded a definitive result.

The theoretical analysis of $\pi\pi$ interactions at low energies is intimately linked to the development of chiral quantum chromodynamics perturbation theory (ChPT) [12–14]. In this approach, the fact that standard QCD perturbation theory is not directly applicable at low energies because the strong coupling becomes large, is circumvented through a systematic expansion of the observables in terms of external momenta and of light quark masses. The spontaneous breakdown of the underlying chiral symmetry is associated with the quark-antiquark vacuum expectation value, the so-called quark condensate $\langle 0|\bar{q}q|0\rangle$. It is normally assumed to be of natural size, or equivalently that the Gell-Mann–Oakes–Renner formula [15] for the pion mass

$$m_\pi^2 \simeq \frac{1}{F_\pi^2}(m_u + m_d)\langle 0|\bar{q}q|0\rangle \tag{1}$$

has only small corrections. Here $F_\pi \simeq 93$ MeV is the pion decay constant. This assumption does not have to be made, as the authors of a less restrictive version of chiral perturbation theory (GChPT) [16,17] pointed out. The measurement of the $\pi\pi$ threshold parameters has been advocated as one of the areas where a significant difference between the two approaches could be observed. ChPT, however, makes firm pre-

*Now at Rutgers University, Piscataway, NJ 08855.
†Now at The Prediction Co., Santa Fe, NM 87505.
‡Now at Albert-Ludwigs-Universität, D-79104 Freiburg, Germany.
§Now at University of Connecticut, Storrs, CT 06269.
‖Now at LIGO/Caltech, Pasadena, CA 91125.
¶Now at SCIPP, University of California, Santa Cruz, CA 95064.

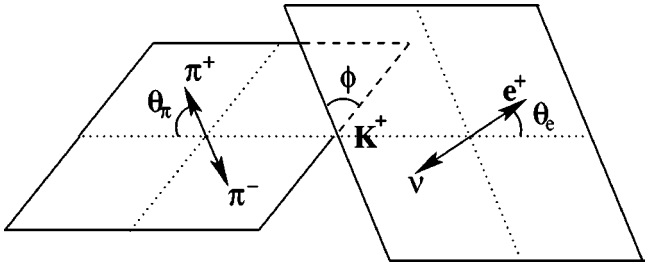

FIG. 1. Kinematic quantities used in the analysis of K_{e4} decay.

dictions for the scattering length. The tree level calculation [$\mathcal{O}(p^2)$ [18]] yields $a_0^0=0.156$ (in this paper we use units of m_π^{-1} for the scattering length). The one-loop [$\mathcal{O}(p^4)$, $a_0^0=0.201\pm0.01$ [19]] and the two-loop calculation [$\mathcal{O}(p^6)$, $a_0^0=0.217$ [20]] show satisfactory convergence. The most recent calculation [21,22] matches the known chiral perturbation theory representation of the $\pi\pi$ scattering amplitude to two loops [20] with the dispersive representation that follows from the Roy equations [23,24], resulting in the prediction $a_0^0=0.220\pm0.005$. The high precision of this prediction has to be contrasted with the experimental value $a_0^0=(0.26\pm0.05)$ extracted from the Geneva-Saclay experiment [9] using the Roy equations and some peripheral $\pi N\to\pi\pi N$ data [25].

The form factors appearing in the weak hadronic current in the K_{e4} decay matrix element have also been extensively used for the determination of the parameters of the ChPT Hamiltonian [26,27]. This program would clearly benefit from lower experimental uncertainties.

II. THEORETICAL BACKGROUND FOR THE ANALYSIS OF K_{e4} DECAY

A. Kinematics

The decay

$$K^+(p)\to\pi^+(p_1)\pi^-(p_2)e^+(p_e)\nu_e(p_\nu) \tag{2}$$

can most conveniently be treated [28] by using three reference frames, as illustrated in Fig. 1: (1) the K^+ rest system (Σ_K), (2) the $\pi^+\pi^-$ rest system ($\Sigma_{\pi\pi}$) and (3) the $e^+\nu_e$ rest system ($\Sigma_{e\nu}$). The kinematics of the K_{e4} decay are then fully described by five variables, introduced by Cabibbo and Maksymowicz [29]:

(1) $s_\pi=M_{\pi\pi}^2$, the invariant mass squared of the dipion.

(2) $s_e=M_{e\nu}^2$, the invariant mass squared of the dilepton.

(3) θ_π, the angle of the π^+ in $\Sigma_{\pi\pi}$ with respect to the direction of flight of the dipion in Σ_K.

(4) θ_e, the angle of the e^+ in $\Sigma_{e\nu}$ with respect to the direction of flight of the dilepton in Σ_K.

(5) ϕ, the angle between the plane formed by the two pions and the corresponding plane formed by the two leptons.

It is useful for the following discussion to introduce the combinations P, Q and L of the momentum four vectors p_1, p_2, p_e and p_ν defined in Eq. (2) and two scalar products derived from them

$$P=p_1+p_2,\ \ Q=p_1-p_2,\ \ L=p_e+p_\nu, \tag{3}$$

$$Q^2=4m_\pi^2-s_\pi,\ \ P\cdot L=\frac{1}{2}(m_K^2-s_\pi-s_e), \tag{4}$$

$$X=[(P\cdot L)^2-s_\pi s_e]^{1/2},\ \ \sigma_\pi=(1-4m_\pi^2/s_\pi)^{1/2}. \tag{5}$$

B. Matrix element

The matrix element is written as

$$M=\frac{G_F}{\sqrt{2}}V_{us}^*\overline{u}(p_\nu)\gamma_\mu(1-\gamma_5)v(p_e)(V^\mu-A^\mu). \tag{6}$$

The vector current V^μ and the axial vector current A^μ have to be Lorentz invariant four-vectors:

$$A^\mu=\frac{1}{m_K}(FP^\mu+GQ^\mu+RL^\mu),$$

$$V^\mu=\frac{H}{m_K^3}\epsilon^{\mu\nu\rho\sigma}L_\nu P_\rho Q_\sigma. \tag{7}$$

The kaon mass m_K was inserted to make the form factors F, G, R and H dimensionless complex functions of $p_1\cdot p_2$, $p_1\cdot p$ and $p_2\cdot p$ or equivalently of s_π, s_e and θ_π.

C. Decay rate

The decay rate following from the matrix element given in Eq. (6) and neglecting terms proportional to m_e^2/s_e is given by [30]

$$d\Gamma_5=\frac{G_F^2V_{us}^2}{2^{12}\pi^6m_K^5}X\sigma_\pi J_5(s_\pi,s_e,\theta_\pi,\theta_e,\phi)\times ds_\pi ds_e d(\cos\theta_\pi)d(\cos\theta_e)d\phi, \tag{8}$$

$$\begin{aligned}J_5=&I_1+I_2\cos2\theta_e+I_3\sin^2\theta_e\cos2\phi\\&+I_4\sin2\theta_e\cos\phi+I_5\sin\theta_e\cos\phi+I_6\cos\theta_e\\&+I_7\sin\theta_e\sin\phi+I_8\sin2\theta_e\sin\phi\\&+I_9\sin^2\theta_e\sin^2\phi.\end{aligned} \tag{9}$$

Again neglecting terms proportional to m_e^2/s_e the functions I_i are given by

$$I_1=\frac{1}{8}\{2|F_1|^2+3(|F_2|^2+|F_3|^2)\sin^2\theta_\pi\}, \tag{10}$$

$$I_2=-\frac{1}{8}\{2|F_1|^2-(|F_2|^2+|F_3|^2)\sin^2\theta_\pi\},$$

$$I_3=-\frac{1}{4}\{|F_2|^2-|F_3|^2\}\sin^2\theta_\pi,\ \ I_4=\frac{1}{2}\mathrm{Re}(F_1^*F_2)\sin\theta_\pi,$$

$$I_5 = -\mathrm{Re}(F_1^* F_3)\sin\theta_\pi, \quad I_6 = -\mathrm{Re}(F_2^* F_3)\sin^2\theta_\pi,$$

$$I_7 = -\mathrm{Im}(F_1^* F_2)\sin\theta_\pi, \quad I_8 = \frac{1}{2}\mathrm{Im}(F_1^* F_3)\sin\theta_\pi,$$

$$I_9 = -\frac{1}{2}\mathrm{Im}(F_2^* F_3)\sin^2\theta_\pi.$$

The form factors F, G, and H are contained in the functions F_i, which are given by

$$F_1 = XF + \sigma_\pi (P\cdot L)\cos\theta_\pi \cdot G,$$
$$F_2 = \sigma_\pi (s_\pi s_e)^{1/2} G, \tag{11}$$
$$F_3 = \sigma_\pi X (s_\pi s_e)^{1/2} \frac{H}{m_K^2}.$$

The contribution of the form factor R is suppressed by a factor m_e^2/s_e and is therefore negligible. Consequently R cannot be determined from K_{e4} decay.

D. Parametrization of the form factors

As noted above, the form factors F, G and H are functions of θ_π, s_π and s_e, and can be determined directly from a fit to the experimental data for sufficiently small bins of these kinematic variables. Alternatively a parametrization recently introduced by Amorós and Bijnens [31] may be used, which is based on a partial wave expansion in the variable θ_π:

$$F = [f_s + f_s' \; q^2 + f_s'' q^4 + f_e(s_e/4m_\pi^2)]e^{i\delta_0^0(s_\pi)} + \tilde{f}_p(\sigma_\pi X/4m_\pi^2)\cos\theta_\pi e^{i\delta_1^1(s_\pi)},$$
$$G = [g_p + g_p' q^2 + g_e(s_e/4m_\pi^2)]e^{i\delta_1^1(s_\pi)}, \tag{12}$$
$$H = (h_p + h_p' q^2)e^{i\delta_1^1(s_\pi)},$$

where $q = [(s_\pi - 4m_\pi^2)/4m_\pi^2]^{1/2}$ is the pion momentum in $\Sigma_{\pi\pi}$. This parametrization was constrained by theoretical models and the expected accuracy of the experimental data. It yields 10 new dimensionless form factor parameters f_s, f_s', f_s'', f_e, $\tilde{f}_p$, g_p, g_p', g_e, h_p, and h_p', which do not depend on any kinematic variables, plus two phase shifts, which can be identified using Watson's theorem [32] with the s and p wave (isoscalar and isovector, respectively) $\pi\pi$ scattering phase shifts δ_0^0 and δ_1^1, which are still functions of s_π. In our analysis we will additionally assume $f_e = \tilde{f}_e = g_e = h_p' = 0$. The validity of this assumption will be experimentally tested. When Eq. (12) is inserted into Eq. (11) and then into Eq. (10), it can be observed that the phase shift difference $\delta = \delta_0^0 - \delta_1^1$ enters via $\cos\delta$ into the terms I_1, I_2, I_4, I_5, and via $\sin\delta$ into the terms I_7 and I_8. Since $\delta < 0.3$ with $\cos\delta > 0.95$ holds in K_{e4} decay, and the kinematic factors suppress the term I_8, only the term I_7 is really relevant, which appears in the decay rate [Eq. (9) and Eq. (8)] multiplied by $\sin\phi$. I_7 and I_8 are the only odd ϕ terms. Hence, as noted by Shabalin [1], and Pais and Treiman [30], the asymmetry of the ϕ distribution is the observable that is most sensitive to the phase shifts. This also holds for any other parametrization of the form factors. The amplitude of the asymmetry is quite small compared to the ϕ independent part, as Figs. 6 and 9 illustrate. This explains why a very high statistics data sample is needed for an accurate measurement of the phase shift difference.

E. $\pi\pi$ scattering length

To establish a relation between the phase shift δ_0^0 and the scattering length normally the analytical properties of the $\pi\pi$ scattering amplitudes and crossing relations are used, which lead to dispersion relations contained in the Roy equations [23]. Ananthanarayan *et al.* [24] have recently updated earlier treatments [33], which were used in the analysis of $\pi\pi$ scattering data, and solved these equations numerically. Their analysis made use of a phase shift parametrization originally proposed by Schenk [34]:

$$\tan\delta_\ell^I = \sqrt{1 - \frac{4m_\pi^2}{s_\pi}}\; q^{2\ell}\{A_\ell^I + B_\ell^I q^2 + C_\ell^I q^4 + D_\ell^I q^6\} \times \left(\frac{4m_\pi^2 - s_\ell^I}{s_\pi - s_\ell^I}\right). \tag{13}$$

The solution of the Roy equations implies that the parameters s_ℓ^I, A_ℓ^I, B_ℓ^I, etc. can be expressed as a function of only two parameters or subtraction constants, which are identified as the $I=0$ and $I=2$ s-wave scattering lengths a_0^0 and a_0^2. For example, the first two coefficients of this expression for the $I=\ell=0$ case read as follows [35]:

$$A_0^0 = a_0^0,$$
$$B_0^0 = 0.2395 + 0.9237\Delta a_0^0 - 3.352\Delta a_0^2 + 0.2817(\Delta a_0^0)^2 + 6.335(\Delta a_0^2)^2 + 6.074\Delta a_0^0 \Delta a_0^2 + \ldots,$$
$$s_0^0 = 36.83 m_\pi^2 (1 + 0.2764\Delta a_0^0 - 0.1409\Delta a_0^2 + \ldots) \simeq (0.847)^2 \;\mathrm{GeV}^2,$$

where $\Delta a_0^0 \equiv a_0^0 - 0.220$ and $\Delta a_0^2 \equiv a_0^2 + 0.0444$. Although K_{e4} decay allows only $I=0$ and $I=1$ contributions, the use of the crossing relations brings in a modest dependence on the $I=2$ scattering length. The $I=1$ phase shifts at low energies are dominated by the ρ resonance and are furthermore small in the region of interest for K_{e4}.

It was recognized by Morgan and Shaw [36] that the possible values of a_0^0 and a_0^2 are restricted to a band in the $a_0^0 - a_0^2$ plane, the so-called *universal band*. This band is defined as the area which is allowed by $\pi\pi$ scattering data above 0.8 GeV [37,38] and the Roy equations. The allowed range, estimated in the most recent analysis [24], is shown in Fig. 10. The central curve of this band is given by

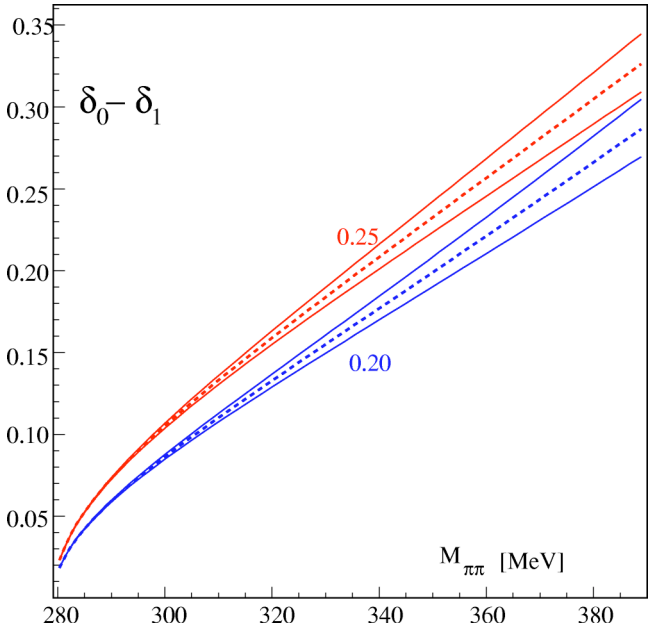

FIG. 2. (Color online) Predictions for the phase shift δ resulting from Eq. (13) and Eq. (14) for two values of a_0^0. The three curves refer to the upper and lower limit and the center, respectively, of the universal band in the (a_0^2, a_0^0) plane [Eq. (14)].

$$a_0^2 = -0.0849 + 0.232 a_0^0 - 0.0865 (a_0^0)^2 [\pm 0.0088], \tag{14}$$

where the figure given in the bracket indicates the width of the band. Figure 2 illustrates the influence of the *universal band* and how the phase shift difference $\delta = \delta_0^0 - \delta_1^1$ depends on the scattering length a_0^0.

It has recently been shown by Colangelo *et al.* [22,39] that the width of the allowed band can be considerably reduced to $[\pm 0.0008]$, if chiral symmetry constraints are imposed in addition. a_0^2 and a_0^0 are then related as

$$\Delta a_0^2 = 0.236 \Delta a_0^0 - 0.61 (\Delta a_0^0)^2 - 9.9 (\Delta a_0^0)^3, \tag{15}$$

where Δa_0^2 and Δa_0^0 have been defined above. This band is also depicted in Fig. 10 with the label CLG.

In ChPT up to order $\mathcal{O}(p^4)$ the scattering lengths are linked to two coupling constants ℓ_3 and ℓ_4. For example, ℓ_3 determines the size of the first order correction to the Gell-Mann–Oakes–Renner relation [Eq. (1)] [15], and is assumed to be *a priori* unknown in GChPT. Colangelo *et al.* [22,39] have argued, that both a_0^0 and a_0^2 can be made dependent solely on ℓ_3, if the scalar radius of the pion is used as an additional input to give a relation between ℓ_3 and ℓ_4. This also holds in GChPT, and Eq. (15) results, when ℓ_4 is eliminated. Once the scattering lengths are known experimentally, a constraint for ℓ_3 and consequently for the quark condensate can be derived.

III. EXPERIMENTAL SET UP

A. Apparatus

The analysis outlined here is based on data recorded at the Brookhaven Alternate Gradient Synchrotron (AGS) in a dedicated run at reduced beam intensity in 1997, employing the E865 detector. The apparatus, described in great detail in [40], is shown in Fig. 3. Here we will mention only its main features. The detector was located in a 6 GeV unseparated beam of approximately 1.5×10^7 K^+ accompanied by about 3×10^8 π^+ and protons per machine spill of 1.6–2.8 s duration. About 6% of the kaons accepted by the beam line decayed in the 5 m long evacuated decay volume. The decay products were separated by charge and swept away from the beam by a first dipole magnet. Negatively charged particles were deflected to the left. A second dipole magnet sandwiched between four proportional wire chambers (P1-P4) served as the spectrometer. The wire chambers, each consisting of four wire planes, were deadened in the region where the beam passed. This arrangement yielded a momentum resolution of $\sigma_P \simeq 0.003\ P^2$ GeV/c, where P, the momentum of the decay products in GeV/c, had a typical range of 0.6 to 3.5. Pions and muons were distinguished from positrons and electrons using two Čerenkov counters, C1 and C2, situated inside and behind the second dipole magnet, and rendered insensitive in the beam region. Both Čerenkov counters, when filled with CH_4 at atmospheric pressure, yielded on average seven photoelectrons, and hence ensured an electron identification probability greater than 99%. An electromagnetic calorimeter of the Shashlyk design [41], located downstream of P4 further aided the separation of the positrons from other charged decay products. It consisted of 30 modules in the horizontal and 20 modules in the vertical direction, but for the beam region, where 6×3 modules were absent. Module size was 11.4 cm high and 11.4 cm wide perpendicular to the beam direction and 15 radiation length deep. The calorimeter was followed by an array of 12 muon chambers, separated by iron planes, employed to discriminate pions against muons. Four hodoscopes were added to the detector for trigger purposes. The A hodoscope was situated just upstream of the calorimeter, the B- and C-hodoscopes were embedded in the muon stack, and the D-hodoscope was located between the first two proportional wire chambers. The detector was completed by a pixel

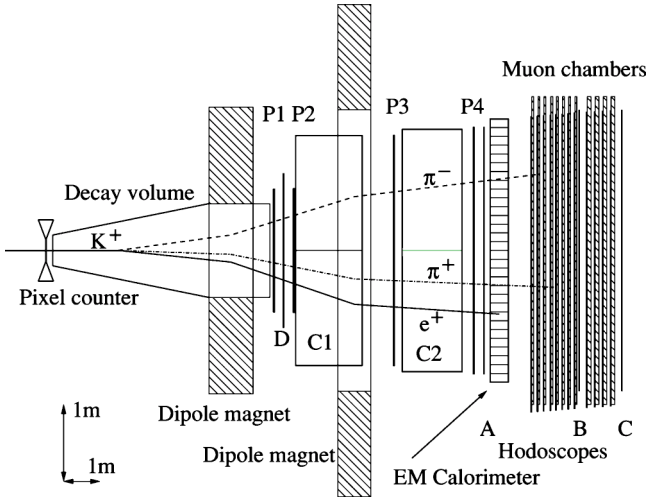

FIG. 3. Plan view of the E865 detector. A K_{e4} event is superimposed.

TABLE I. Experimental resolutions for the five kinematic variables used in the analysis.

Variable	FWHM	
s_π	0.00133	GeV^2
s_e	0.00361	GeV^2
θ_π	0.147	rad
θ_e	0.111	rad
ϕ	0.404	rad

counter, installed just upstream of the decay volume, which measured the position of the incoming kaons. This device consisted of an array of 12 (horizontally) by 32 (vertically) scintillating pixels, each with an area of 7×7 mm^2.

Table I summarizes the resolution of the apparatus in the five variables required to describe the kinematics of the K_{e4} decay.

B. Trigger requirements

The trigger was designed as a multilevel structure with increasing sophistication. The lowest trigger level (T0) indicated the presence of three charged particle tracks, two on the right and one on the left side, each signaled by a coincidence between the A counter and the corresponding calorimeter module directly behind it ($\mathrm{A}\cdot\mathrm{SH}$). For each combination of coincidences on the right only a limited, kinematically acceptable region on the left was allowed. To ensure that the trigger resulted from particles coming from the decay volume, at least one coincidence on both sides between the D-counter and $\mathrm{A}\cdot\mathrm{SH}$ was required. The next trigger level (T1) demanded the presence of a positron in order to reject events from the $K^+\rightarrow\pi^+\pi^+\pi^-$ (K_τ) decay, and dismissed all events with evidence for the presence of an electron to eliminate events from $K^+\rightarrow\pi^+\pi^0$ ($\pi^0\rightarrow e^+e^-\gamma$, K_{dal}) decay, both rather common decay modes. Consequently, this trigger level required signals in both Čerenkov counters on the right (corresponding to at least 2.5 photoelectrons) and vetoed all events with a signal in either Čerenkov counters on the left (at least 0.25 photoelectrons). The final trigger level (T2) rejected events with a high occupancy in the wire chambers, most likely caused by noise in the read-out electronics. It did not reject many events, but the ones it rejected would have required an exceedingly large amount of computer time in the reconstruction. In addition to K_{e4} candidates, a few prescaled monitor triggers were also recorded, e.g. a minimum bias trigger (T0 without the T1 requirement) dominated by accidentals and K_τ events, and a trigger sensitive to K_{dal} events, used to check the Čerenkov counter efficiency [40].

IV. K_{e4} EVENT SELECTION AND ANALYSIS

A. Reconstruction

The kinematic reconstruction of an event, described in detail in [40], proceeded as follows: In the first step raw wire hits in the proportional chambers were combined to space points, requiring signals in at least three of the four wire planes in a chamber. Then the space points were combined to tracks. A track was found if at least three chambers contributed with a space point each. Next, employing a measured map of the magnetic field in the dipole magnets, the momenta of the tracks were fitted. For events with at least three reconstructed tracks, a fitting algorithm, again utilizing the field map, determined the decay vertex as the position from which the distance s to the three tracks was minimal. For events containing more than three tracks, the combination that produced the lowest s was tagged as the most probable set of track candidates from kaon decay. Finally, the kaon direction was obtained from the hit in the pixel counter and the vertex. The kaon momentum could then be fitted by tracing the kaon back through the beam line to the production target 27.5 m upstream of the decay tank. In the last reconstruction step the particle identification information was assigned to the tracks found.

B. Selection

K_{e4} candidates had to pass the following selection criteria: a vertex within the decay tank of acceptable quality s, a momentum reconstructed from the three daughter particles below the beam momentum, a timing spread between the signals caused by the tracks in the A hodoscope and the calorimeter consistent with the resolution of 0.5 ns. Finally we required an unambiguous identification of the e^+, assured by light in the appropriate photomultiplier tubes in both Čerenkov counters and an energy loss in the calorimeter consistent with the momentum of the track, and of the π^-, secured by the absence of a signal above the noise in the Čerenkov counters and an energy loss in the calorimeter consistent with that of a minimum ionizing particle or a hadron shower. The cuts described above ensured K_{e4} events of good quality, but the resulting event sample still contained a considerable amount of background events.

C. Backgrounds

The major background contributions came from K_τ decay and accidentals. A K_τ could fake a K_{e4} by either (1) a misidentification of one of the π^+ as a positron due to δ rays, noise in the photomultiplier tubes or the presence of an additional parasitic positron, or (2) a decay of a π^+ directly or via a μ^+ into an e^+. The dominating accidental background arose from combinations of a π^+ and a π^- originating from a K_τ decay with a positron from either the beam or from a K_{dal} decay (2-1 accidental from K_τ).

To reject background from K_τ decay, we required that the kaon reconstructed from the three charged daughter particles did not track back to the target, using the fact that the reconstruction for K_{e4} is incomplete due to the undetected neutrino. The remaining K_τ background can be made visible by plotting the K_{e4} candidates under the K_τ hypothesis, i.e. assigning to the positron a pion mass. The K_τ background appears as a narrow peak sitting on the broad distribution originating from K_{e4} decays, as seen in Fig. 4(a).

Accidentals of the 2-1 type from K_τ are characterized by (1) the positron track tends to be out of time in the A-hodoscope and the calorimeter compared with the two

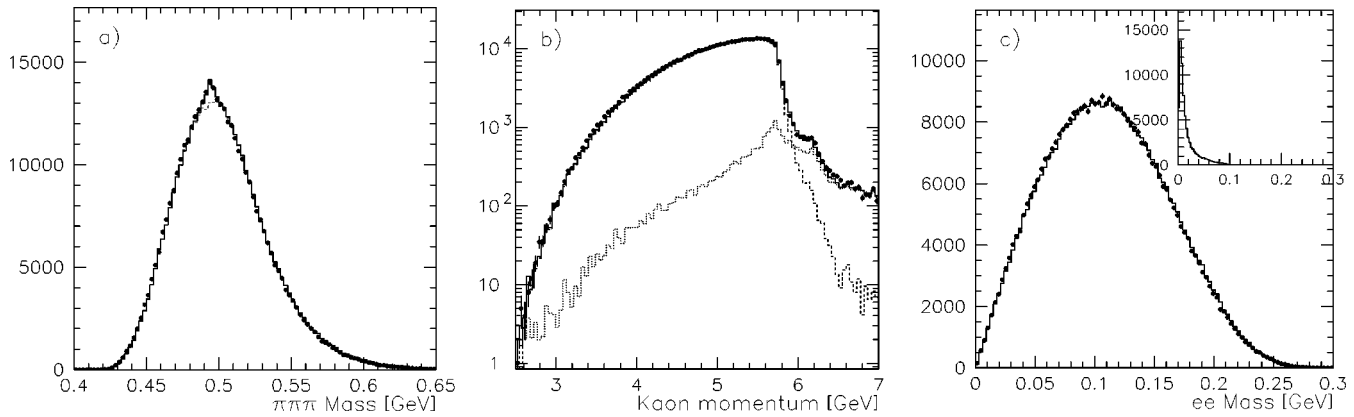

FIG. 4. Background contributions: the markers show the data while the solid histogram displays the Monte Carlo simulation. (a) Three-pion invariant mass distribution for K_{e4} candidate events, assigning a pion mass to the positron. The small peak at the K^+ mass arises from K_τ events. (b) Total momentum reconstructed from the three charged track momenta. The solid histogram is the sum of the Monte Carlo simulation of K_{e4} events (dashed histogram) and the background from 2-1 accidentals (lower dotted histogram). (c) Electron-positron invariant mass M_{ee} assigning electron mass to the reconstructed π^- for K_{e4} events. K_{dal} events (inset) are characterized by low values of M_{ee}.

pion tracks; (2) the distance of closest approach between the positron track and each pion track is typically larger than the distance between the two pions; (3) the position of the vertex along the beam axis tends to be more upstream in K_τ and hence also in 2-1 accidentals from K_τ compared with K_{e4}, due to smaller average transverse momentum; (4) in the calorimeter more clusters of energy are found, due to the possibility of two decays in the same time window. These characteristics were used to construct a likelihood function in order to suppress 2-1 accidentals. The remaining background can be exposed by inspecting the distribution of the total visible momentum in the event, reconstructed from the sum of the three charged particle momenta. Accidentals of the 2-1 type display a large tail above the beam momentum, as is demonstrated in Fig. 4(b). The agreement between data and the sum of Monte Carlo and background indicates that this background is well understood. For the background simulation we used K_τ monitor events with a fourth accidental positron track. The uncertainty in the evaluation of this background under the signal region below the beam momentum yields the largest contribution to the systematic error of the background estimate.

The excellent particle identification capabilities of our apparatus reduce the background originating from K_{dal} decay, where the e^- gets misidentified as a π^-, to a negligible level. This can be made evident by plotting the invariant mass M_{ee} of the electron-positron pair, assigning the electron mass to the π^- [Fig. 4(c)]. This distribution shows no enhancement at the low values of M_{ee} characteristic for K_{dal} events.

Table II summarizes the background rates.

D. Final sample

After applying the event selection criteria described above, 406,103 events remained, of which we estimate $388{,}270 \pm 5025$ to be K_{e4} events. This corresponds to an increase in statistics by more than a factor of 10 compared with previous experiments.

V. MONTE CARLO SIMULATION

A good Monte Carlo simulation of the detector is a necessary ingredient for the analysis of the decay distributions and the determination of the absolute branching ratio. This simulation starts with the kaon beam at the upstream end of the decay tank with a spatial and momentum distribution deduced from our ample supply of K_τ^+ monitor events, for which the incident K^+ can be fully reconstructed. The K^+ is then allowed to decay in a preselected mode along its trajectory in the decay tank. To model the physics of the K_{e4} decay, initial values of the matrix elements were chosen in accordance with the ChPT analysis at the one loop level [42,43] of the Geneva-Saclay experiment [9]. Radiative corrections are included following Diamant-Berger [44] (see also Sec. VII below). For the decay modes K_τ and K_{dal},

TABLE II. Compilation of fraction of background events. 1-1-1 accidentals: accidental combinations of two independent pion tracks and a positron track; 2-1 accidentals: combinations of two pions from a K_τ with an accidental positron or combinations of a π^+ and a positron from a K_{dal} decay with an accidental π^-; $^{[a]}$ $\pi^0 \to e^+e^-\gamma$ and e^- misidentification.

Background	Fraction
K_τ with π^+ misidentification	$(1.3 \pm 0.3) \times 10^{-2}$
K_τ with $\pi^+ \to e^+ \nu_e$	$(3.5 \pm 0.2) \times 10^{-3}$
K_τ with $\pi^+ \to \mu^+ \nu_\mu$ and $\mu^+ \to e^+ \nu_e \overline{\nu_\mu}$	$(2.6 \pm 0.3) \times 10^{-3}$
$K^+ \to \pi^0 \pi^{+[a]}$	$(2.5 \pm 0.6) \times 10^{-5}$
$K^+ \to \pi^0 e^+ \nu_e^{[a]}$	$(0.4 \pm 0.1) \times 10^{-5}$
$K^+ \to \pi^0 \mu^+ \nu_\mu^{[a]}$	$(0.4 \pm 0.1) \times 10^{-5}$
$K^+ \to \pi^+ \pi^0 \pi^{0[a]}$	$(0.3 \pm 0.1) \times 10^{-5}$
1-1-1 accidentals	$(0.9 \pm 0.4) \times 10^{-4}$
2-1 accidentals from K_τ	$(2.4 \pm 1.2) \times 10^{-2}$
2-1 accidentals from K_{dal}	$(0.9 \pm 0.4) \times 10^{-3}$

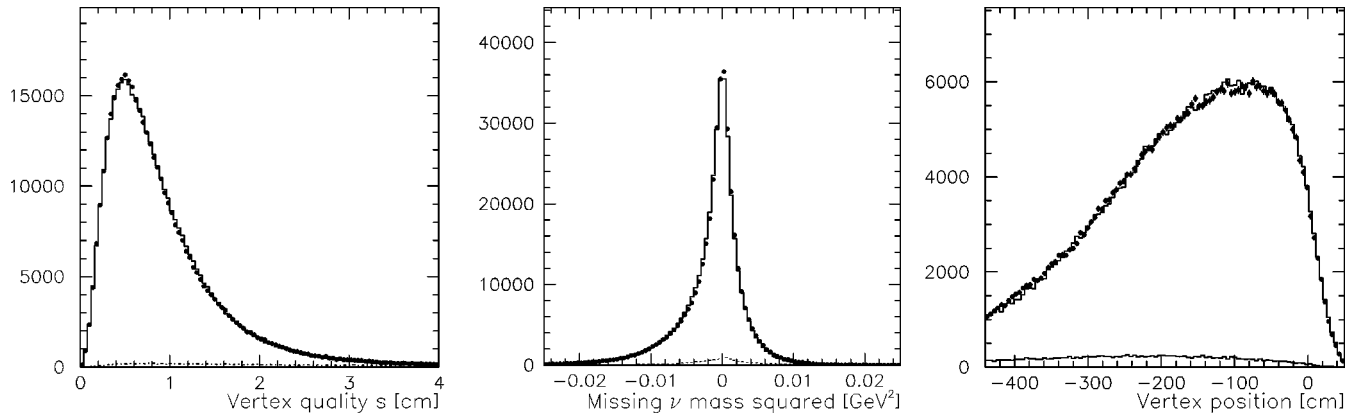

FIG. 5. Comparison of the Monte Carlo simulation (histogram) with data (markers with error bars). Left: distance of closest approach s to the common vertex for the three charged tracks; center: missing neutrino mass squared; right: distribution of decay vertices along the beam direction z ($z=0$ at the entrance of the first dipole magnet). The dashed histograms show the background contributions.

needed for the determination of the branching ratio and the evaluation of the background, we use the matrix elements given in Refs. [45] and [46]. The detector response is handled with a GEANT-based [47] simulation of the E865 apparatus, and the simulated events are processed through the same reconstruction and selection programs as data events. With these tools, we generated 81.6×10^6 K_{e4} events, resulting in 2.9×10^6 accepted events, about 7.5 times more than data events. The quality of the simulation is demonstrated in Fig. 5, which displays the vertex quality s, the missing neutrino mass squared, and the position of the vertex along the beam axis as examples. The vertex quality is a crucial quantity in the event reconstruction; the missing neutrino mass squared is sensitive to the resolution; and the vertex position depends on the decay matrix element and detector acceptance. The good agreement between data and Monte Carlo indicates that ChPT describes the data well and that our event selection procedure did not introduce a significant bias. We also compare Monte Carlo with data distributions for the kinematically very distinct K_τ and K_{dal} decays, getting again a nice agreement (see, e.g. [40]). Furthermore, we find that the K_{dal} branching ratio is consistent with the published value [48], using K_τ as normalization channel. This underlines the good understanding of the geometrical acceptance and the efficiency of the various detector elements.

VI. BRANCHING RATIO

The K_{e4} branching ratio was normalized with respect to the K_τ decay. As mentioned in Sec. III B, we collected K_τ events in a minimum bias trigger concurrently with K_{e4} events. K_τ is the most common kaon decay with three charged particles in the final state, which strongly simplifies the selection of a clean sample of events. To identify K_τ events, we require the reconstruction of a vertex, as for K_{e4}, and the reconstruction of the kaon mass. With $BR(\tau)=5.59\pm0.05\%$ [48], the K_{e4} branching ratio BR and the decay rate λ are calculated as

$$BR(K_{e4})=BR(K_\tau)\frac{N(K_{e4})A(K_\tau)}{N(K_\tau)A(K_{e4})}C$$

$$\begin{aligned} N(K_{e4})[N(K_\tau)] &= \text{number of } K_{e4}[K_\tau] \text{ events} \\ &= 388{,}270\pm5025[1.487\times10^9] \\ A(K_{e4})[A(K_\tau)] &= \text{acceptance for } K_{e4}\ [K_\tau] \text{ events} \\ &= 3.77\%\ [10.29\%] \end{aligned} \tag{16}$$

$$\begin{aligned} C &= \text{accidental veto correction} \\ &= 1.0312\pm0.0022, \end{aligned}$$

leading to

$$\begin{aligned} BR(K_{e4}) &= (4.109\pm0.008\pm0.110)\times10^{-5} \\ \lambda(K_{e4}) &= (3321\pm6\pm89)\,\mathrm{s}^{-1}. \end{aligned} \tag{17}$$

The first error is statistical, the second is systematic. The result is in good agreement with previous experiments, as is evident from Table III. The systematic errors are summarized in Table IV. The dominant contributions are from the background subtraction and Čerenkov countereefficiencies. The error in the background subtraction results from the uncertainty in the background rate for 2-1 accidentals from K_τ, as mentioned in Sec. IV C. The efficiency of the Čerenkov counters was determined using K_{dal} decays, collected with the special purpose Čerenkov counter trigger described in Sec. III B. The uncertainty results from the fact that K_{dal} events populate phase space areas different from K_{e4}. This is mainly significant on the beam right side, where 2.5 photoelectrons are required to identify a positron. The branching ratio includes radiative K_{e4} events, i.e. $K^+\to\pi^+\pi^-e^+\nu_e\gamma$, since no cut on the missing neutral mass squared is made. Diamant-Berger [44] found that the ratio of radiative to nonradiative K_{e4} events for photon energies above 30 MeV is only $(1.0\pm0.5)\%$. A small fraction of these, which lead to

TABLE III. K_{e4} branching ratios measured in older experiments.

Reference	No. of events	Branching ratio
PDG [48]		$(3.91\pm0.17)\times10^{-5}$
Rosselet *et al.* [9]	30318	$(4.03\pm0.17)\times10^{-5}$
Beier *et al.* [8]	8141	
Bourquin *et al.* [7]	1609	$(4.11\pm0.38)\times10^{-5}$
Schweinberger *et al.* [6]	115	$(3.91\pm0.50)\times10^{-5}$
Ely *et al.* [5]	269	$(3.26\pm0.35)\times10^{-5}$
Birge *et al.* [4]	69	$(3.74\pm0.84)\times10^{-5}$

an additional cluster in the calorimeter could be rejected, because the number of clusters is used in the likelihood function for background rejection.

VII. FITS TO THE DECAY DISTRIBUTIONS

In pursuing the goal of determining the form factors and $\pi\pi$ scattering phase shifts, three different approaches have been followed, which have been outlined in Sec. II D. The K_{e4} form factors F, G, and H, and the phase shift δ can be directly extracted for a conveniently chosen grid of bins in the kinematic variables. This approach makes no assumption on the analytical behavior of these quantities. In the second approach, the parametrization of Eq. (12) is used and the phase shifts are related to the two scattering lengths using Eq. (13). This allows use of the whole data sample in a single fit. Finally, either Eq. (14) or Eq. (15) can be used in addition, reducing the number of parameters by one. The statistical method which we describe below is the same for all three approaches.

TABLE IV. Systematic errors in the branching ratio measurement.

Sources	σ_{BR}/BR
Background subtraction	0.012
K_τ prescale factor	0.0076
Magnetic field map	0.005
Čerenkov counterinefficiencies	0.015
PWC efficiencies	0.006
Fiducial volume	0.005
Track quality	0.0022
Vertex reconstruction	0.0016
Z position of vertex	0.0012
Tracking back to target	0.0019
Timing cuts	0.0020
e^+ identification in the calorimeter	0.0007
π^- identification	0.0011
2-1 accidental likelihood	0.0006
K_{e4} matrix element (statistics)	0.006
K_τ mass resolution	0.0081
K_τ branching ratio	0.009
Total (added quadratically)	0.0268

A. Data treatment

The experimental distributions must be fit to Eq. (8), taking into account the acceptance and resolution of the apparatus, with the form factors and phase shifts as free parameters. Following the recommendations by Eadie [49] we select equi-probable bins for each kinematic variable, namely six bins in s_π, five in s_e, ten in $\cos\theta_\pi$, six in $\cos\theta_e$, and 16 bins in ϕ. With a total of 28,800 bins there are on average 13 events in each bin.

Following the procedure used by the Geneva-Saclay experiment [9,44], we minimize a χ^2 function defined as

$$\chi^2 = 2\sum_j n_j \ln\left[\frac{n_j}{r_j}\left(1-\frac{1}{m_j+1}\right)\right] + 2\sum_j (n_j+m_j+1)\ln\left[\frac{1+\frac{r_j}{m_j}}{1+\frac{n_j}{m_j+1}}\right], \quad (18)$$

where the sum runs over all bins. n_j, r_j and m_j are the number of data events, expected events and generated Monte Carlo events in bin j, respectively. This χ^2 is deduced from the probability

$$P(n,m,r) = \int_0^\infty \int_0^\infty e^{-u}\frac{u^n}{n!}e^{-v}\frac{v^m}{m!}\delta\left(u-\frac{r}{m}v\right)dudv$$

and takes into account the limited number of Monte Carlo events. It reduces to the more familiar expression

$$\chi^2 = \sum_j [2(r_j-n_j)+2n_j\ln(n_j/r_j)]$$

for large m_j.

The expected number of events r_j is calculated to be

$$r_j = Br(K_{e4})\frac{N^K}{N^{MC}}\sum \frac{J_5(F,G,H)^{new}}{J_5(F,G,H)^{MC}}, \quad (19)$$

where the sum runs over all Monte Carlo events in bin j. N^K is the number of K^+ decays derived from the number of K_τ events. N^{MC} is the number of generated events. $J_5(F,G,H)^{MC}$ [Eq. (9)] is evaluated at the relevant set of kinematic variables for the simulated event with the form factors F, G, and H calculated at $q=q^{MC}$. $J_5(F,G,H)^{new}$ is evaluated with the same kinematic set and F, G, H recalculated from the parameters of the fit. Thus, we apply the parameters on an event by event basis, and at the same time, we divide out a possible bias caused by the matrix element, making the fit independent of the ChPT ansatz used to generate the Monte Carlo events.

B. Fit of the decay rate in multiple bins in s_π

For the fit in multiple bins two further assumptions are being made, namely that the form factors do not depend on s_e and that the form factor F contributes to s waves only.

TABLE V. Form factors and phase shifts for the six bins in dipion invariant mass $M_{\pi\pi}$ (in units of 10^{-3}). $\langle M_{\pi\pi}\rangle$ refers to the centroid of the bin. The number of degrees of freedom (NDF) for each fit is 4796. The first errors are statistical, the second systematic. The fourth quantity, which is in parentheses, indicates the shift of the central value of the parameter which resulted from the application of the radiative corrections. F, G and H given here are the moduli of the complex form factor defined in Eq. (12).

$M_{\pi\pi}$, $\langle M_{\pi\pi}\rangle$ (MeV)	280–294, 285.2	294–305, 299.5	305–317, 311.2
F	$5832\pm13\pm80$ (-26)	$5875\pm14\pm83$ $(+34)$	$5963\pm14\pm90$ $(+44)$
G	$4703\pm89\pm69$ $(+22)$	$4694\pm62\pm67$ $(+27)$	$4772\pm54\pm70$ $(+34)$
H	$-3740\pm800\pm180$ (-59)	$-3500\pm520\pm190$ (-50)	$-3550\pm440\pm200$ (-167)
$\delta=\delta_0^0-\delta_1^1$	$-16\pm40\pm2$ $(+0.5)$	$68\pm25\pm1$ (-0.4)	$134\pm19\pm2$ (-1.3)
χ^2/NDF	1.071	1.080	1.066
$M_{\pi\pi}$, $\langle M_{\pi\pi}\rangle$ (MeV)	317–331, 324.0	331–350, 340.4	>350, 381.4
F	$6022\pm16\pm94$ $(+46)$	$6145\pm17\pm96$ $(+45)$	$6196\pm20\pm83$ $(+34)$
G	$5000\pm51\pm82$ $(+38)$	$5003\pm49\pm83$ $(+31)$	$5105\pm50\pm74$ $(+31)$
H	$-3630\pm410\pm230$ (-177)	$-1700\pm410\pm240$ (-160)	$-2230\pm480\pm330$ (-173)
$\delta=\delta_0^0-\delta_1^1$	$160\pm17\pm2$ $(+0.1)$	$212\pm15\pm3$ $(+0.2)$	$284\pm14\pm3$ $(+0.6)$
χ^2/NDF	1.103	1.093	1.034

This is equivalent to setting f_e, g_e and $\tilde{f}_p$ equal to zero in the parametrization of Ref. [31]. The validity of these assumptions will be discussed in Sec. VII C below. Hence the four parameters F, G, and H and $\delta\equiv\delta_0^0-\delta_1^1$ are fit for each of the six bins in $M_{\pi\pi}=\sqrt{s_\pi}$. Table V summarizes the results. Figure 6 shows the ϕ distribution for each of the bins, which illustrates the high quality of the fit.

The centroids $\langle M_{\pi\pi}\rangle$ of the bins are estimated following the recommendations by Lafferty and Wyatt [50]. The dominant systematic error for F, G, and H has the same origin as that of the branching ratio measurement. The major contributions to the systematic error of δ are the subtraction of the background, and resolution effects, i.e. deviations between the original and reconstructed kinematics.

We have also included the full magnitude of the radiative corrections in the systematic error. As mentioned above in Sec. V, we have calculated these corrections using formulas given in Refs. [44,51] based on the work of Neveu and Scherk [52]. Basically one has to consider two types of radiative corrections, those where a real photon is radiated by one of the charged particles involved in the decay and those where a virtual photon is exchanged between two charged particles. The former are dominated by inner bremsstrahlung in particular of the positron [44], as e.g. experimentally determined in the related decay $K^0_{Le3}\to\pi^\pm e^\mp\overline{\nu}_e(\nu_e)$ [53]. The Low theorem [54] ensures that off-shell effects appear only in second order and hence modifications of the hadronic form factors are expected to be negligible. The Coulomb interaction of the charged particles in the decay, however, has noticeable effects, in particular its most important contribution, the mutual attraction of the pion pair, as already observed in the Geneva-Saclay experiment [9,44]. The repulsion or attraction between the positron, kaon and the two pions, which we also included, is unimportant. As an example we have reproduced the $\pi\pi$ Coulomb attraction below [51], which we have used to reweight each event:

$$d\Gamma_T=d\Gamma_0(1+\alpha C), \tag{20}$$

where

$$C=\pi\frac{1+v^2}{2v}+\frac{2}{\pi}\ln\left(\frac{2E_m}{m_\pi}\right)\left[\frac{1+v^2}{2v}\ln\left(\frac{1+v}{1-v}\right)-1\right]+\frac{1}{\pi}\left(\frac{2+v^2}{2v}\right)\ln\left(\frac{1+v}{1-v}\right)+\frac{8A}{\pi}\left(\frac{1+v^2}{2v}\right)-\frac{1}{4\pi},$$

and

$$A=\int_0^{0.5\ln((1+v)/(1-v))} z\coth z\,dz$$

$$=\mathcal{L}_2(v)-\mathcal{L}_2(-v)-\frac{1}{2}\left[\mathcal{L}_2\left(\frac{2}{1+v}\right)-\mathcal{L}_2\left(\frac{2}{1-v}\right)\right],$$

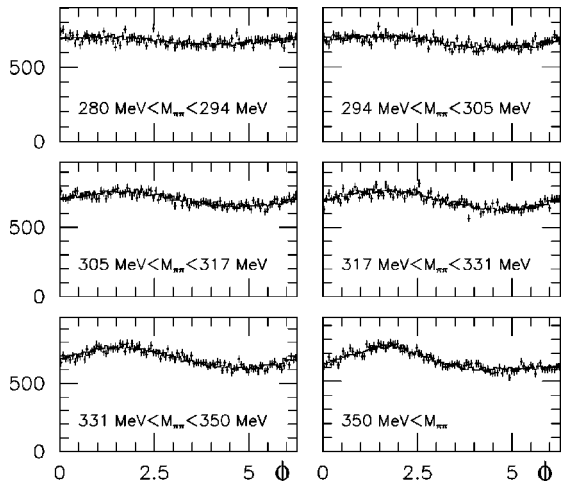

FIG. 6. ϕ distributions for the six bins in $M_{\pi\pi}$. The markers with error bars represent the data, the histogram the modified Monte Carlo distribution after the fit.

TABLE VI. Form factors and scattering length a_0^0 in the parametrization of Eq. (12) using either Eq. (14) or Eq. (15). The results for the form factor parameters are identical for both fits. The first error is statistical, the second systematic. The quantity in parentheses is the shift in the result of the parameter which resulted from the radiative corrections.

f_s	$5.75\pm0.02\pm0.08$ (-0.03)
f_s'	$1.06\pm0.10\pm0.40$ $(+0.37)$
f_s''	$-0.59\pm0.12\pm0.40$ (-0.37)
g_p	$4.66\pm0.05\pm0.07$ $(+0.03)$
g_p'	$0.67\pm0.10\pm0.04$ (±0.00)
h_p	$-2.95\pm0.19\pm0.20$ (-0.16)
a_0^0	$0.228\pm0.012\pm0.004$ (±0.000) [Eq. (14)]
a_0^0	$0.216\pm0.013\pm0.004$ (±0.000) [Eq. (15)]
(χ^2/NDF)	30963/28793

$$\mathcal{L}_2(x)\equiv-\int_0^x\frac{1}{y}\ln|1-y|dy.$$

Here v is the velocity of the pions in the dipion center-of-mass system (in units of c), α the fine-structure constant, and E_m a cut-off energy fixed at 30 MeV. In all tables where results are given (Tables V, VI, VII and VIII) we have listed the effect of applying the radiative corrections separately. While the form factors F and G and the phase shifts δ are nearly unaffected, the form factor H changes between 1.5 and 9.4%.

The small deviation of χ^2/NDF from the expected value of one may reflect the discreteness of the background. The number of background events which we add to the generated events is smaller than the number of bins, and the background is distributed over almost the whole phase space. By using tighter cuts, which reduce the background contributions by a factor of two, we have confirmed that the results for the form factors and phase shifts remain unchanged.

The results from Table V allow us to examine the s_π dependence of the form factors F, and G, and of the phase δ, which are displayed in Figs. 7 and 8. For the various fits to these data, which we report below, the value of χ^2/NDF is always below one. Following Amorós and Bijnens [31], we fitted F with a second degree polynomial, while a linear function suffices for G, with the following results:

$$f_s=5.77\pm0.10,\ \ f_s'=0.95\pm0.58,\ \ f_s''=-0.52\pm0.61,$$

$$g_p=4.68\pm0.09,\ \ g_p'=0.54\pm0.20. \tag{21}$$

TABLE VII. Results from the fits, where the form factors parameters $\tilde{f}_p$, f_e, and g_e were allowed to vary one at a time. The quantity in parentheses shows the influence of radiative corrections.

Parameters	Value	χ^2/NDF
$\tilde{f}_p$	$-0.34\pm0.10\pm0.27$ (-0.02)	30952/28792
f_e	$-0.32\pm0.10\pm0.24$ $(+0.02)$	30954/28792
g_e	$0.04\pm0.34\pm0.88$ (±0.00)	30963/28793

TABLE VIII. Fit of form factor parameters and scattering lengths a_0^0 and a_0^2. The first error is statistical, the second systematic. The quantity in parentheses shows the influence of the radiative corrections.

f_s	$5.75\pm0.02\pm0.08$ (-0.03)
f_s'	$1.06\pm0.10\pm0.40$ $(+0.37)$
f_s''	$-0.60\pm0.12\pm0.40$ (-0.37)
g_p	$4.65\pm0.48\pm0.07$ $(+0.03)$
g_p'	$0.69\pm0.11\pm0.04$ $(\pm\ 0.00)$
h_p	$-2.95\pm0.19\pm0.20$ (-0.16)
a_0^0	$0.203\pm0.033\pm0.004$ (-0.001)
a_0^2	$-0.055\pm0.023\pm0.003$ (-0.001)
χ^2/NDF	30963/28792

Figure 7 also shows the results of a linear fit: $F(q)=F(0)\times(1+\lambda_F q^2)$. We found

$$F(0)=5.83\pm0.08,\ \lambda_F=0.079\pm0.015, \tag{22}$$

where the error of λ_F was calculated using only the relative errors of F in the six bins. These results are in agreement with those of the Geneva-Saclay experiment [9], namely,

$$F(0)=5.59\pm0.14,\ \ \lambda_F=0.08\pm0.02. \tag{23}$$

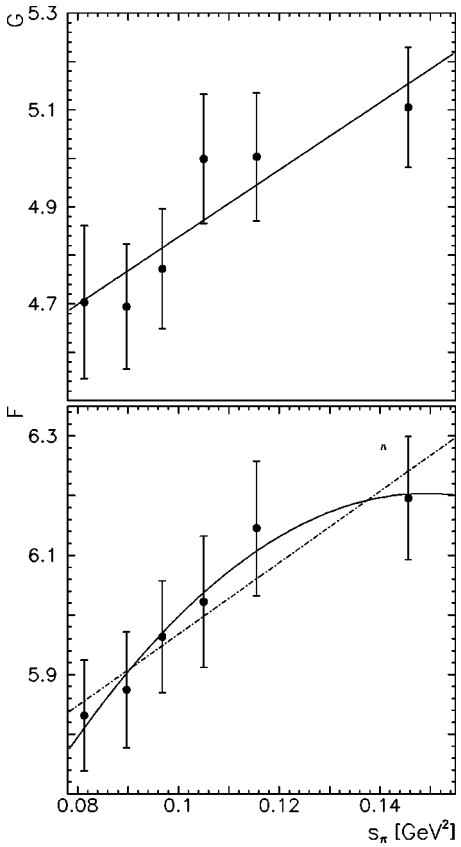

FIG. 7. s_π dependence of form factors F and G.

In the latter analysis it was assumed that $\lambda_F=\lambda_G\equiv g_p'/g_p$ holds, which is confirmed by our analysis, albeit within large error limits.

Good agreement with the previous measurements [9] and considerably improved precision is shown in Fig. 8, where the phase shift difference δ is plotted versus $M_{\pi\pi}=\sqrt{s_\pi}$. A fit using Eq. (13) with relation Eq. (14), taking the central curve of the universal band with the six data points for δ leads to the following value of the scattering length:

$$a_0^0=0.229\pm0.015\ \ (\chi^2/\mathrm{NDF}=4.8/5). \tag{24}$$

The use of Eq. (14) then implies $a_0^2=-0.0363\pm0.0029$.

C. Fits to the whole data set

In this section we list the results of various fits to the whole data sample. A more detailed discussion and comparison will follow in Sec. VIII.

If we substitute the phase shifts δ in Eq. (12) via Eq. (13) and Eq. (14) or Eq. (15) for the relation between a_0^0 and a_0^2, we can use the whole data sample in one single fit, which will yield the scattering length a_0^0, and the six form factor parameters f_s, f_s', f_s'', g_p, g_p', h_p. The remaining form factor parameters f_e, $\tilde{f}_p$, g_e, and h_p' have been fixed at zero. The results which are listed in Table VI are in excellent agreement with the ones derived in the previous paragraph. However, as expected, the statistical errors of the various parameters are smaller. The quality of the fit can be judged from Fig. 9. The agreement between the Monte Carlo simulation modified for the final values of the form factors and phase shifts in all five kinematic variables is very satisfactory.

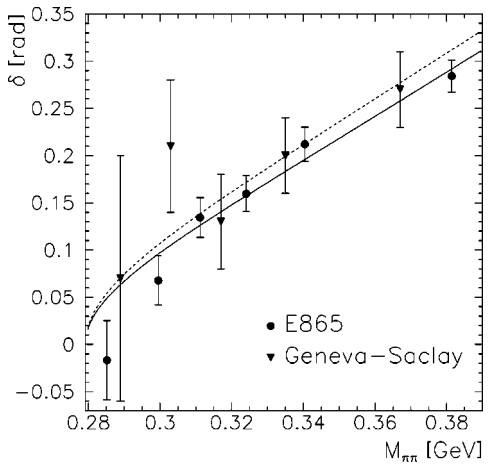

FIG. 8. Phase shift difference δ. The fits are given by Eq. (13) as a function of the scattering length a_0^0. Solid line: this experiment; dashed line: Geneva-Saclay [9].

In all previous fits, we have assumed that the decay rate does not depend on s_e and that there are no contributions from p waves to F. To check this approximation we have allowed these form factors, one at a time, to vary in our fits too for the case where Eq. (14) was used. Table VII shows

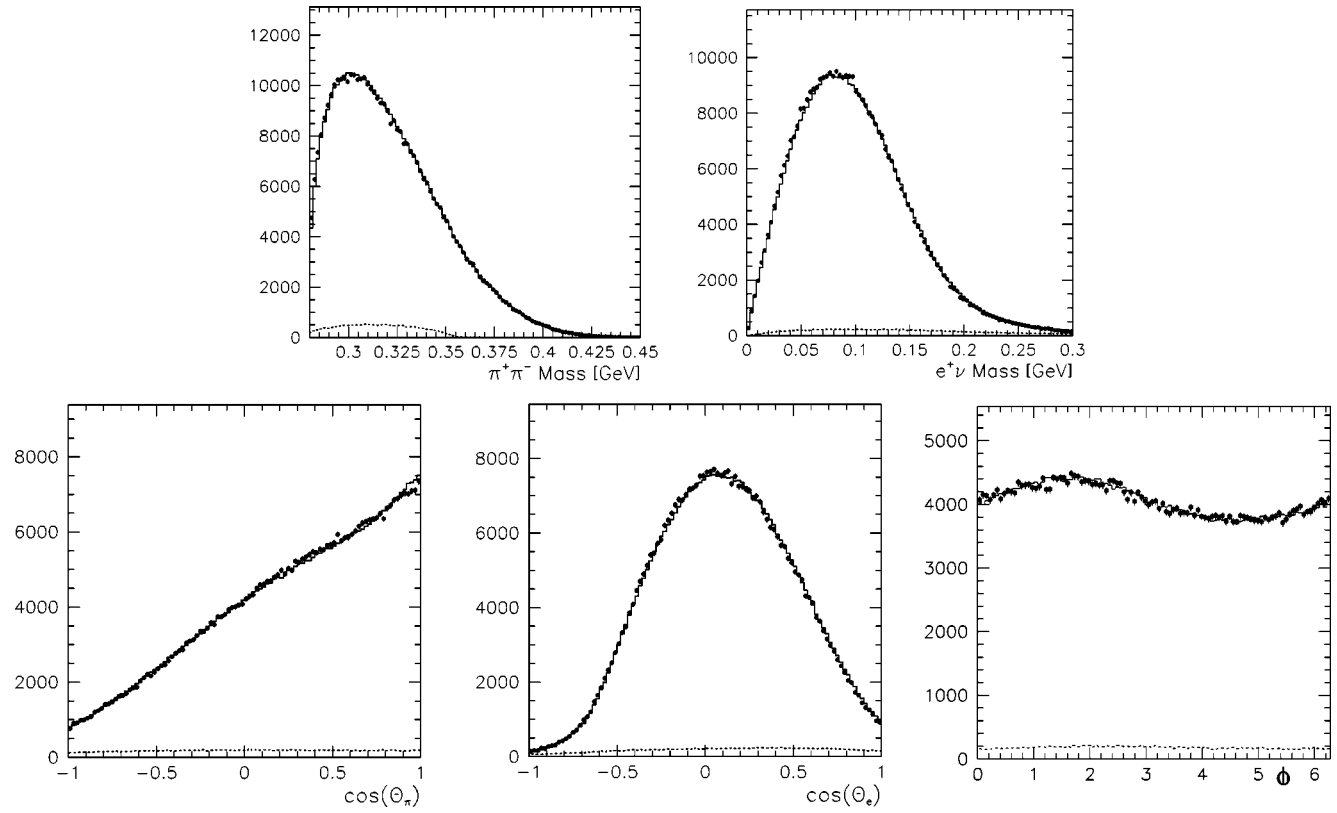

FIG. 9. Invariant masses and angles describing the K_{e4} decay. The histograms are the Monte Carlo distributions while the points with the error bars represent the data. The dashed histograms show the background.

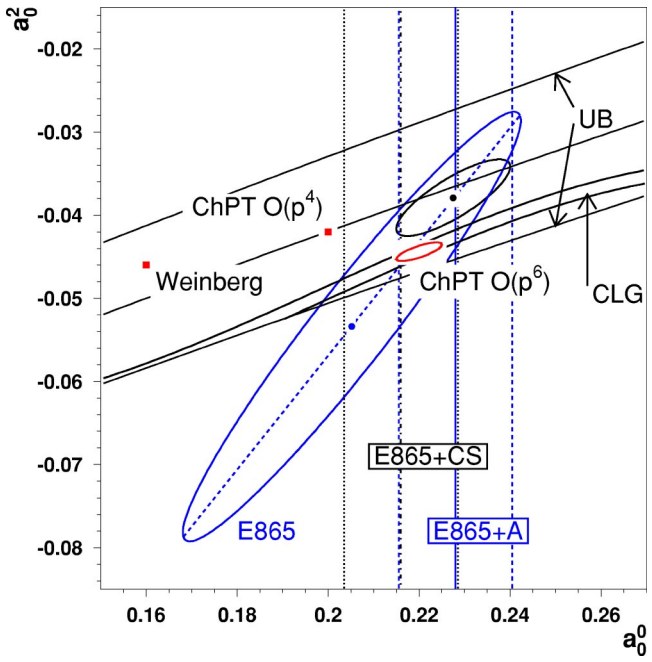

FIG. 10. (Color online) Results for the $\pi\pi$ scattering lengths a_0^0 and a_0^2 obtained from fits to the K_{e4} data directly or from fits to the phase shifts obtained in this experiment. Large ellipse labeled E865: fit to our K_{e4}-data leaving both a_0^2 and a_0^0 as free parameters using Eq. (13) with the parameters of Ref. [24] (1σ contour, see text for remark concerning the region outside the universal band). Medium size ellipse without label: fit of Ref. [55] (1σ contour) to our phase shifts. Theoretical predictions: [18] (Weinberg, square), [19] [ChPT O(p^4), square], and [21] [ChPT O(p^6), small ellipse]. Solid curves labeled UB: universal band of allowed values based on Eq. (14). Solid curves labeled CLG: narrow band of allowed values based on Eq. (15). Solid vertical line labeled E865 (+A $\equiv$ analyticity constraints): fit to K_{e4} data using Eq. (14) with 1 σ error limits given by dashed vertical lines. Dashed-dotted line labeled E865 (+CS $\equiv$ analyticity and chiral symmetry constraints) fit to K_{e4} data using Eq. (15) with 1 σ error limits given by dotted vertical lines.

that all three form factors are found to be consistent with zero. The nominal values of the contributions to the form factors F and G are at the 2% or less level. In all three cases, the dominant contribution to the systematic errors came from the resolution of the missing neutrino mass squared, and a smaller non-negligible error from the background estimate.

In order to assess the sensitivity of our data to a_0^2 directly we have also made a fit to the data where it was allowed to vary independently, rather than being fixed via Eq. (14) or Eq. (15). The result is given in Table VIII and Fig. 10. While the form factor parameters, as was expected, did not change, a_0^0 shifts to a lower value with a larger error bar, which encompasses the values found above. The error ellipse for this fit is shown in Fig. 10. It illustrates the strong correlation between the two scattering lengths. The long axis of this ellipse follows the equation $a_0^2 = -0.1939 + 0.6851 a_0^0$.

VIII. SUMMARY AND DISCUSSION

The main results of this analysis are the measurements of the $\pi\pi$-phase shift difference δ near threshold and of the form factors F, G and H of the hadronic current, and their momentum dependence with a precision which has not been previously attained. We emphasize again that the analysis based on these data in six bins of invariant $\pi\pi$ mass is model independent.

The analysis which directly relates our data to the scattering length a_0^0, on the other hand, depends on additional input, which leads to slightly different results. While there is a consensus [22,55,39] on the use of the Roy equations [24] and Eq. (13) to relate the phase shifts to the scattering lengths, there exist slightly different ways of linking a_0^0 to a_0^2, and how to make use of peripheral $I=2$ data. These differences produce slightly different results for both a_0^2 and a_0^0 with overlapping statistical errors. The experimental and systematic uncertainities for both the phase shifts and scattering lengths are considerably smaller than the statistical ones and are therefore irrelevant to this discussion.

If both a_0^0 and a_0^2 are allowed to vary independently (Table VIII), we obtain a result outside the universal band in the (a_0^0, a_0^2) plane, namely,

$$a_0^0 = 0.203 \pm 0.033, \quad a_0^2 = -0.055 \pm 0.023.$$

Descotes *et al.* [55] have performed a fit to our published phase shifts [10], which are identical to the ones given here, and obtained

$$a_0^0 = 0.237 \pm 0.033, \quad a_0^2 = -0.0305 \pm 0.0226,$$

with a strong correlation between the two values, which we also observe in our result. Only that part of the 1σ error contour of our result (the large ellipse in Fig. 10) which overlaps the universal band is consistent with both our and the $I=2$ data [56,57], and only within this band the solution of the Roy equations [24] used here is valid [58]. From the 1σ contour and its central axis we may deduce how much the results listed in Table VI change if the input assumptions on the relation between a_0^0 and a_0^2 are varied. Using the lower limit of the band defined by the bracket in Eq. (14) we find a shift of a_0^0 by -0.016, while the maximum allowed upward shift inside the 1σ contour and the band is 0.012. Assigning these values as theoretical errors to our result, we obtain

$$a_0^0 = 0.228 \pm 0.012 \text{ stat.} \pm 0.004 \text{ syst.} \, {}^{+0.012}_{-0.016} \text{ theor.} \quad (25)$$

The use of Eq. (14) implies

$$a_0^2 = -0.0365 \pm 0.023 \text{ stat.} \pm 0.008 \text{ syst.} \, {}^{+0.0031}_{-0.0026} \text{ theor.} \quad (26)$$

Since the central curve of the universal band is thought to be the best representation of the $I=2$ data, it is no surprise, that the fit of Descotes *et al.* [55], which used our phase shifts and those of the Geneva-Saclay experiment [9], Eq. (13) with the parametrization of Ref. [24] and the $I=2$ data below 800 MeV [56,57], gave nearly identical results

$$a_0^0 = 0.228 \pm 0.012, \quad a_0^2 = -0.0382 \pm 0.0038. \quad (27)$$

This result is also shown in Fig. 8.

Using the narrower band in the (a_0^2, a_0^0) plane defined by Eq. (15) our result is

$$a_0^0 = 0.216 \pm 0.013 \text{ stat.} \pm 0.004 \text{ syst.} \pm 0.002 \text{ theor.}, \tag{28}$$

which implies

$$a_0^2 = -0.0454 \pm 0.0031 \text{ stat.} \pm 0.0010 \text{ syst.} \pm 0.0008 \text{ theor.}, \tag{29}$$

where the theoretical errors have been evaluated as before and correspond to the width of the band. Descotes *et al.* [55], again fitting to our phase shifts, have obtained for this case

$$a_0^0 = 0.218 \pm 0.013, \quad a_0^2 = -0.0449 \pm 0.0033, \tag{30}$$

again in agreement with our result and also with $a_0^0 = 0.221 \pm 0.026$, obtained by Colangelo *et al.* [39] by direct numerical inversion of the relation between the phase shifts and the scattering lengths.

From this discussion we may deduce first that using our full data sample or the phase shifts, which we have extracted from it, in the six bins in $M_{\pi\pi}$ leads to the same results. This will make further use of our data easy, should theoretical discussion continue and require this. Second, it has become clear that the most probable values of the two scattering lengths extracted from the K_{e4}-data and low-energy $I=2$ data, resting on a minimum of theroretical assumptions given by analyticity and crossing are those given in Eqs. (25) and (26), or Eq. (27). Using the additional constraints implied by chiral symmetry and the value of the scalar radius [22,39] leads to a value of the scattering length consistent within the statistical errors with this result, albeit just 1σ lower. The authors of Ref. [55] have elaborated in detail how their ansatz differs from that of Ref. [39], and what the possible implications, if any, are for the chiral pertubation theory parameters ℓ_3 and ℓ_4 and the size of the quark condensate. In view of the large errors and also inconsistencies in the $I=2$ phase shift data [56,57], it seems premature to assign much significance to this minor discrepancy. Because of the reduced theoretical uncertainties we prefer to quote the values of Eqs. (28) and (29) as our final result. Both solutions for a_0^0 are in very good agreement with the full two-loop standard ChPT prediction [21,22]

$$a_0^0 = 0.220 \pm 0.005, \quad a_0^2 = -0.0444 \pm 0.0010.$$

The influence of the reduced uncertainties of our results on the form factors F, G and H on the determination of the low energy constants of ChPT is evident from recent work of Amorós *et al.* [27], who have updated their earlier work [26] using our data [10]. The constants L_1^r, L_2^r and L_3^r changed from 0.53 ± 0.25, 0.71 ± 0.27 and -2.72 ± 1.12 (in units of 10^{-3}), respectively, to 0.43 ± 0.12, 0.73 ± 0.12 and -2.35 ± 0.37.

The first nonvanishing contribution to the anomalous form factor H in ChPT is predicted to be $H=-2.67$ [59]. This agrees well with our value of $H = -2.95 \pm 0.19 \pm 0.20$. An estimation of the next to leading order gives only a small contribution [60].

ACKNOWLEDGMENTS

We gratefully acknowledge the contributions to the success of this experiment by Dave Phillips, the staff and management of the AGS at the Brookhaven National Laboratory, and the technical staffs of the participating institutions. We also thank J. Bijnens, C. Colangelo, J. Gasser, M. Knecht, H. Leutwyler, and J. Stern for many fruitful discussions. This work was supported in part by the U.S. Department of Energy, the National Science Foundations of the U.S., Russia, and Switzerland, and the Research Corporation.

[1] E.P. Shabalin, Zh. Éksp. Teor. Fiz. **44**, 765 (1963) [Sov. Phys. JETP **17**, 517 (1963)].
[2] E.L. Koller *et al.*, Phys. Rev. Lett. **9**, 328 (1962).
[3] L.B. Okun, and E.P. Shabalin, Zh. Éksp. Teor. Fiz. **37**, 1775 (1959) [Sov. Phys. JETP **10**, 1252 (1960)].
[4] R.W. Birge *et al.*, Phys. Rev. **139**, 1600 (1965).
[5] R.P. Ely *et al.*, Phys. Rev. **180**, 1319 (1969).
[6] W. Schweinberger *et al.*, Phys. Lett. **36B**, 246 (1971).
[7] M. Bourquin *et al.*, Phys. Lett. **36B**, 615 (1971); P. Basile *et al.*, *ibid.* **36B**, 619 (1971); A. Zylberstein *et al.*, *ibid.* **38B**, 457 (1972).
[8] E.W. Beier *et al.*, Phys. Rev. Lett. **29**, 511 (1972); **30**, 399 (1973).
[9] L. Rosselet *et al.*, Phys. Rev. D **15**, 574 (1977).
[10] S. Pislak *et al.*, Phys. Rev. Lett. **87**, 221801 (2001).
[11] DIRAC Collabration, F. Gomez *et al.*, in Proceedings of the International Euroconference on Quantum Chromodynamics: 15 Years of the QCD, Montpellier, France, 2000 [Nucl. Phys. B (Proc. Suppl.) **96**, 259 (2001)].
[12] S. Weinberg, Physica A **96**, 327 (1979); J. Gasser and H. Leutwyler, Ann. Phys. (N.Y.) **158**, 142 (1984); Nucl. Phys. **B250**, 465 (1985).
[13] For a recent brief overview see, e.g., H. Leutwyler, in QCD@Work: International Conference on Quantum Chromodynamics: Theory and Experiment, edited by Pietro Colangelo and Giuseppe Nardulli, AIP Conf. Proc. No. 602 (AIP, Melville, NY, 2001); hep-ph/0107332.
[14] ''Effective Field Theories of QCD,'' Proceeding of the 264th WE-Heraeus Seminar, Bad Honnef, Germany, 2001, edited by J. Bijnens, U.G. Meißner, and A. Wirzba, hep-ph/0201266, and references therein.
[15] M. Gell-Mann, R.J. Oakes, and B. Renner, Phys. Rev. **175**, 2195 (1968).
[16] N.H. Fuchs, H. Sazdjian, and J. Stern, Phys. Lett. B **269**, 183 (1991).
[17] M. Knecht, B. Moussalam, J. Stern, and N.H. Fuchs, Nucl. Phys. **B457**, 513 (1995); **B471**, 445 (1996).
[18] S. Weinberg, Phys. Rev. Lett. **17**, 616 (1966).

[19] J. Gasser and H. Leutwyler, Phys. Lett. **125B**, 325 (1983).
[20] J. Bijnens *et al.*, Phys. Lett. B **374**, 210 (1996); Nucl. Phys. **B508**, 263 (1997); **B517**, 639 (1998).
[21] C. Colangelo *et al.*, Phys. Lett. B **488**, 261 (2000).
[22] G. Colangelo, J. Gasser, and H. Leutwyler, Nucl. Phys. **B603**, 125 (2001).
[23] S.M. Roy, Phys. Lett. **36B**, 353 (1971).
[24] B. Ananthanarayan *et al.*, Phys. Rep. **353**, 207 (2001).
[25] M.M. Nagels *et al.*, Nucl. Phys. **B147**, 189 (1979).
[26] G. Amorós, J. Bijnens, and P. Talavera, Phys. Lett. B **480**, 71 (2000); Nucl. Phys. **B585**, 293 (2000); **B598**, 665 (2001)
[27] G. Amorós, J. Bijnens, and P. Talavera, Nucl. Phys. **B602**, 87 (2001).
[28] For a recent discussion see J. Bijnens, C. Colangelo, G. Ecker, and J. Gasser, in *The Second DAPHNE Physics Handbook*, edited by L. Maiani, G. Pancheri, and N. Paver (INFN-LNF-Divisione Ricerca, SIS-Uffico Publicazioni, Frascati, 1995), p. 315, hep-ph/9412392.
[29] N. Cabibbo and A. Maksymowicz, Phys. Rev. **137**, B438 (1965).
[30] A. Pais and S.B. Treiman, Phys. Rev. **168**, 1858 (1968).
[31] G. Amorós and J. Bijnens, J. Phys. G **25**, 1607 (1999).
[32] K.M. Watson, Phys. Rev. **88**, 1163 (1952).
[33] For a review see D. Morgan and M.R. Pennington, in *The Second DAPHNE Physics Handbook* [28], p. 193.
[34] A. Schenk, Nucl. Phys. **B363**, 97 (1991).
[35] The numerical values for the coefficients are listed in Ref. [24], Appendix D, and Ref. [55], Appendix B.
[36] D. Morgan and G. Shaw, Nucl. Phys. **B10**, 261 (1969).
[37] B. Hyams *et al.*, Nucl. Phys. **B64**, 134 (1973).
[38] S.D. Protopopescu *et al.*, Phys. Rev. D **7**, 1279 (1973).
[39] G. Colangelo, J. Gasser, and H. Leutwyler, Phys. Rev. Lett. **86**, 5008 (2001).
[40] R. Appel *et al.*, Nucl. Instrum. Methods Phys. Res. A **479**, 349 (2002).
[41] G.S. Atoyan *et al.*, Nucl. Instrum. Methods Phys. Res. A **320**, 144 (1992).
[42] J. Bijnens, Nucl. Phys. **B337**, 635 (1990).
[43] C. Riggenbach *et al.*, Phys. Rev. D **43**, 127 (1991).
[44] A.M. Diamant-Berger, Ph.D. thesis, University of Paris, Orsay, Centre d'Etudes Nucléaires de Saclay, 1976, report CEA-N-1918.
[45] See T.G. Trippe, in Groom *et al.* [48], p. 503.
[46] K.O. Mikaelian and J. Smith, Phys. Rev. D **5**, 1763 (1972).
[47] R. Brun *et al.*, GEANT 3.21, CERN, Geneva.
[48] Particle Data Group, D.E. Groom *et al.*, Eur. Phys. J. C **15**, 1 (2000); Particle Data Group, K. Hagiwara *et al.*, Phys. Rev. D **66**, 010001 (2002).
[49] W.T. Eadie *et al.*, *Statistical Methods in Experimental Physics* (North Holland, Amsterdam, 1971).
[50] G.D. Lafferty and T. R. Wyatt, Nucl. Instrum. Methods Phys. Res. A **355**, 541 (1995).
[51] See Ref. [44], Appendix 2.
[52] A. Neveu and J. Scherk, Phys. Lett. **27B**, 384 (1968).
[53] A. Alavi-Harati *et al.*, Phys. Rev. D **64**, 112004 (2001).
[54] F. Low, Phys. Rev. **110**, 974 (1958).
[55] S. Descotes, N.H. Fuchs, L. Girlanda, and J. Stern, Eur. Phys. J. C **24**, 469 (2002).
[56] W. Hoogland *et al.*, Nucl. Phys. **B69**, 266 (1974); **B126**, 109 (1977).
[57] M.J. Losty *et al.*, Nucl. Phys. **B69**, 185 (1974).
[58] We thank G. Colangelo for pointing this out.
[59] J. Wess and B. Zumino, Phys. Lett. **37B**, 95 (1971).
[60] L. Ametller *et al.*, Phys. Lett. B **303**, 140 (1993).